Monthly Notices
of the
ROYAL ASTRONOMICAL SOCIETY

MNRAS **493,** 1204–1216 (2020) doi:10.1093/mnras/staa201

Global Site Selection for Astronomy

N. Aksaker,[1,2★] S. K. Yerli,[3] M. A. Erdoğan,[4] Z. Kurt,[2,5] K. Kaba,[6] M. Bayazit[5] and C. Yesilyaprak[6,7]

[1]*Adana Organized Industrial Zone Vocational School of Technical Science, University of Çukurova, 01410 Adana, Turkey*
[2]*Space Science and Solar Energy Research and Application Center (UZAYMER), University of Çukurova, 01330 Adana, Turkey*
[3]*Department of Physics, Orta Doğu Teknik Üniversitesi, 06800 Ankara, Turkey*
[4]*Landscape Architecture Department, Faculty of Architecture, Hatay Mustafa Kemal University, 31060 Hatay, Turkey.*
[5]*Remote Sensing and Geographic Information System, University of Çukurova, 01330 Adana, Turkey*
[6]*Astrophysics Research and Application Center (ATASAM), Atatürk University, 25240 Erzurum, Turkey*
[7]*Department of Astronomy and Astrophysics, Science Faculty, Atatürk University, 25240 Erzurum, Turkey*

Accepted 2020 January 20. Received 2020 January 20; in original form 2019 December 5

ABSTRACT

A global site selection for astronomy was performed with 1 km spatial resolution (∼1 gigapixel in size) using long-term and up-to-date datasets to classify the entire terrestrial surface of the Earth. Satellite instruments are used to get the following datasets of geographical information system (GIS) layers: cloud coverage, digital elevation model, artificial light, precipitable water vapour, aerosol optical depth, wind speed, and land use and land cover. A multi-criteria decision analysis (MCDA) technique is applied to these datasets, creating four different series where each layer will have a specific weight. We introduce for the first time a suitability index for astronomical sites (SIAS). This index can be used to find suitable locations and to compare different sites or observatories. The midwestern Andes in South America and the Tibetan Plateau in western China were found to be the best in all SIAS series. Considering all the series, less than 3 per cent of all terrestrial surfaces are found to be the best regions to establish an astronomical observatory. In addition to this, only approximately 10 per cent of all current observatories are located in good locations in all SIAS series. Amateurs, institutions or countries aiming to construct an observatory could create a shortlist of potential site locations using a layout of SIAS values for each country without spending time and budget. The outcomes and datasets of this study have been made available through a website, the Astro GIS Database, at www.astrogis.org.

Key words: methods: data analysis – methods: observational – site testing.

1 INTRODUCTION

Constructing an astronomical observatory hosting a telescope is an engineering application with cost efficiency in mind. However, the main reason to have a protected telescope is to collect and focus as many photons as possible without being disturbed by the atmosphere or light sources not originating from space. Therefore, astronomers have been trying to find the best locations so that their investments in telescope time could become cost efficient when the number of clear nights goes above 90 per cent annually, corresponding to almost eleven months. At the moment, the best observatory sites are highly telescope populated. However, they are not great in number. So, while the Thirty Meter Telescope (TMT, 30 m) and the European Extremely Large Telescope (E-ELT, 39 m) are being built on these kind of sites, the future of ground-based astronomy is based on finding more of the best of the best sites (Sarazin, Graham & Kurlandczyk 2006; Schöck et al. 2009). On other hand, the demand for small- to medium-sized dedicated telescopes has always been on the rise, simply because the first concern is to collect photons for each question asked by the astronomers. Therefore, the demand for *suitable* sites for each telescope and observatory pair will continue to be an important topic for both astronomers and engineers.

Astronomers have been walking the path of *observation* for many decades with science and technology working hand to hand to support them. Therefore, this path has to be simplified for both observers and engineers by finding an answer to the following question: How does one choose and/or build an observatory with all the required constraints involved in the question to be answered?

In the last decade, an empirical relation between the cost (C) and size (D) of the telescope has been widely used:

$$C \sim D^{\alpha} \quad (1)$$

★ E-mail: naksaker@cu.edu.tr

where D is the aperture of the telescope in metres. Due to improvements in technology within the past decade, the value α has decreased from 2.7 to 2.0 (van Belle, Meinel & Meinel 2004). Therefore, it is safe to assume that almost every institution or organization could find required budget to have their questions answered with their own instruments under an observatory constructed on a *suitable* observatory site.

Even though there is no official list of observatories with all the mandatory properties listed, the unofficial list with simple details contains more than 2000 observatories (one recent number is ∼2122, as shown in Fig. 1). In addition to this, due to the nature of astronomy, observers usually do not register their observatories or their instruments unless they are used in scientific campaigns. Therefore, it is easy to assume that in future we would expect to have more and more observatories being built hosting telescopes of varying sizes. However, even though all is well for the technologies used in observatories, statistically and practically it is not the same story for the selection of *observatory sites*. In the past:

(i) Neither observers nor engineers paid much attention to the importance of site selection (see Section 4.1). Note that even in the early years of now mid-sized telescope construction, site testings were not very detailed.

(ii) Atmospheric conditions were not measured, recorded or catalogued as much as needed.

(iii) Due to technological limitations, small-sized telescopes were preferred over costly large telescopes and they were allocated mostly close to the institutions.

Therefore, when site selection is involved in today's ecology of astronomy and engineering, one needs to not spend budget and time over and over again to find just a single *suitable* site for all the constraints involved.

This work attempts to solve the overhead of site selection once and for all globally by using the whole land surface of Earth for amateurs, astronomers, institutions and governments: in general, for anybody who wants to have an idea of the site before starting up a project.

1.1 Site selection

The site-selection procedure is complex due to its nature: data from different sources are combined and analysed together. Tools and techniques for the geographic information system (GIS) have already provided many solutions to these kind of problems, offering cost- and time-efficient solutions to decision makers. Therefore, GIS techniques in site selection are widely used in many fields: hospitals, solar and wind farmsteads and urban solid-waste plants, as well as observatories (Nas et al. 2009; Soltani & Marandi 2011; Uyan 2013; Noorollahi, Yousefi & Mohammadi 2016).

In the case of an astronomical observatory site, another important parameter is the major wavelengths targeted in the scientific rationale of the observatory. Thus, when observations on longer wavelengths, especially in the infrared, are targeted then observers expect to have lower water vapour content in the atmosphere. This can be achieved if precipitable water vapour (PWV) measurements are involved in the selection process (Küçük et al. 2012; Otarola et al. 2019). For radio astronomy, RFI (radio frequency interference) should also be included as a layer as well as PWV (Umar, Zainal Abidin & Abidin Ibrahim 2014). Note also that a recent site-testing study by Otarola et al. (2019) included PWV, temperature and wind data from radiosonde measurements for a limited time span and for a localized region centred mainly on observatory sites. They summarize that PWV and temperature are very important in site selection for radio astronomy; however, a wind vertical profile has to be obtained for the final decision.

Another recent site-selection exercise was carried out for Iran's 3.4 m optical telescope (Nasiri et al. 2019). They used available long-term meteorological and geographical parameters. Similarly, in Pakistan, Daniyal & Hassan Kazmi (2019) conducted a study to identify potential optical telescope sites by using an analytical hierarchy process (AHP) with a multi-criteria decision analysis (MCDA) technique.

The most comprehensive work on global-scale site selection was carried out for the 39 m European Extremely Large Telescope (E-ELT): FriOWL (Sarazin et al. 2006). They used satellite data including various climatological parameters. FriOWL used GIS techniques by including several astroclimatological layers together: monthly mean temperature, outgoing longwave radiation, water vapour, cloud coverage, wind, aerosol index (Graham et al. 2005). Its spatial resolution was around $2.5 \times 2.5°$ (approximately 300×300 km^2). It contains several climatic layers with a time coverage of approximately 15 yr. Since many parameters with many different data types (satellite data, processed ground-based data etc.) were involved together, it was found to be useful even though it has a limited spatial resolution with limited temporal resolution up to the year 2002. However, in the end, it was successfully used for finding the best site for the E-ELT.

Another recent study by Hellemeier et al. (2019), which again uses FriOWL for site testing, compiled astroclimatological data from 15 cites distributed all around the world for a period of 45 yr. They conclude that having a long-term dataset combined with seasonal variation could elevate the importance of the astronomical observatory sites.

Continuous improvements on meteorological models result in lower spatial resolution of the atmospheric layers. One of the latest studies on this kind of modelling was done by Osborn & Sarazin (2018). They applied the European Centre for Medium-Range Weather Forecasts (ECMWF) model successfully in astronomical site testing.

In Table 1, a summary of earlier astronomical site-selection studies by different groups is given along with the GIS layers used. In all these works, two layers are found to be common: cloud coverage and altitude. We also include artificial light (AL) as an important layer because the light pollution in operational observatories becomes more and more invasive.

2 DATASETS

When constructing a data collection for GIS analysis it is always preferable for the layer to cover a long time series. This can easily be achieved when polar-orbiting satellites monitor the Earth from space to the surface. Since their lifetimes are long enough, they will naturally produce long, continuous and consistent databases. The typical date range for such Earth-observing satellites is around five years.

In this study, we have collected the following datasets from different missions and instruments on-board these satellites. Links, websites, resources and repositories of datasets that we downloaded are listed in Table 2. Downloading of the layers is automated using an in-house coded PYTHON script.

Note that the Antarctica continent has been excluded from the analysis because the continent does not have datasets for all layers; it has only CC, DEM and PWV. However, due to the continent's special location, these datasets have to be studied separately. In this continent, CC is expected to be very small on average.

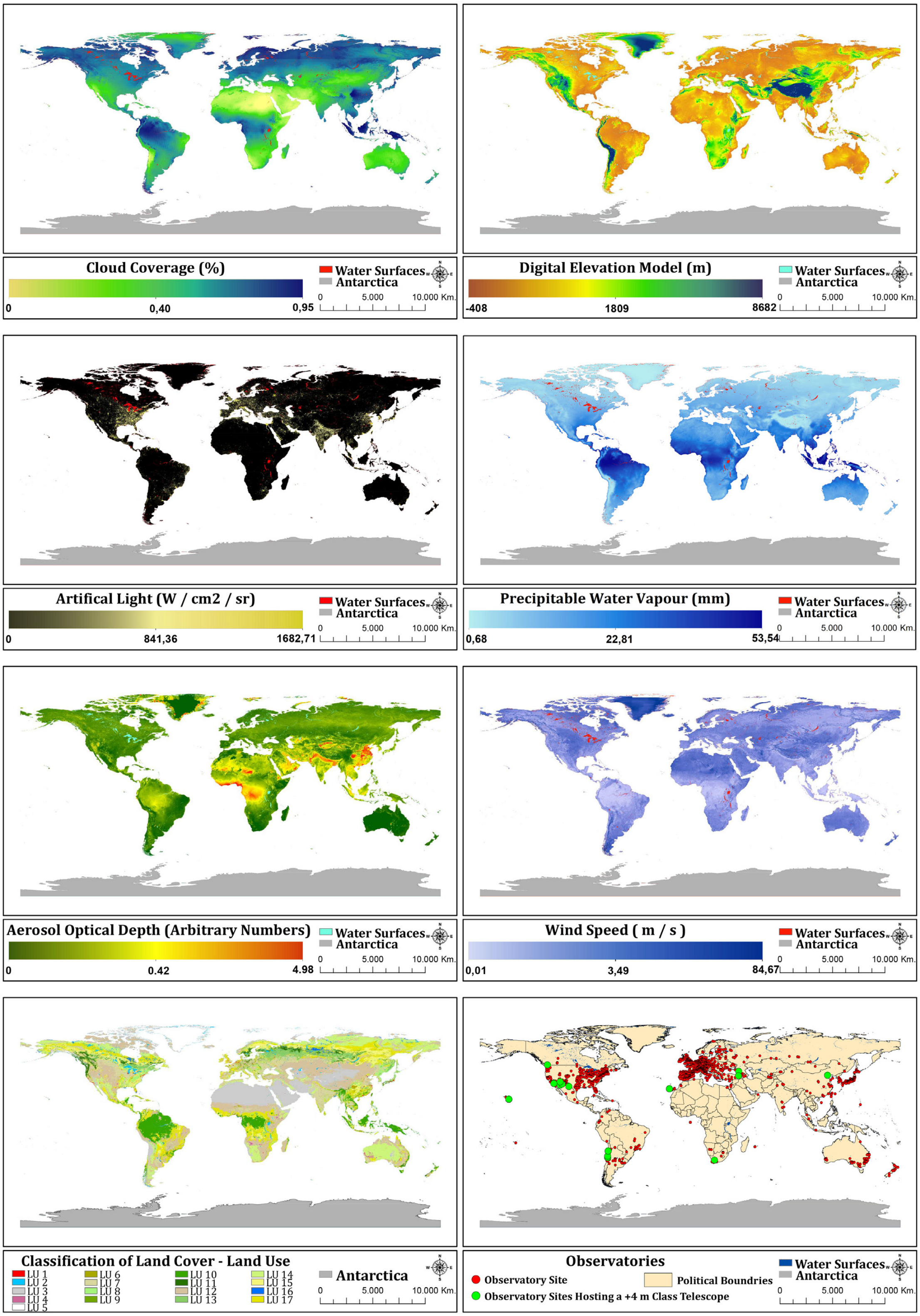

Figure 1. The GIS layers used in this study (from top to bottom): first row: cloud coverage (left), digital elevation model (right); second tow: artificial light (left), precipitable water vapour (right); third row: aerosol optical depth (left), wind speed (right); fourth row: land use and land cover (LULC, left), observatory locations (right). The abbreviations in the LULC layer are taken from table 3 of Sulla Menashe & Friedl (2018). See Section 2 for details.

Table 1. A short summary of earlier works on astronomical site selection. Abbreviations for layers are divided into two: main and others. *Main layers* (marked with 'X' when the layer is used in the reference): DEM: digital elevation model, CC: cloud coverage, AL: artificial light. *Other layers* (in alphabetical order): A: accessibility, AOD: aerosol optical depth, AT: air temperature, AU: aurora, AI: airglow, BL: boundary layer, BP: barometric pressure, D: dewpoint, FS: free seeing, GH: geopotential height, IH: inversion height, IF: inversion frequency, LU: land use, LC: land cover, LS: local specifications, O: orography, OLR: outgoing longwave radiation, OT: optical turbulence, PWV: precipitable water vapour, RH: relative humidity, S: seismicity, SB: sky brightness, SD: sunshine duration, ST: surface temperature, SW: surface wind, TS: terrain slope V: vegetation, VP: vapour pressure, VV: vertical velocities, WD: wind direction, WS: wind speed. Note that MENA is shorthand for the 'Middle East and North Africa'.

Region	Main layers			Other layers	References
	DEM	CC	AL		
Western China	X	X	–	A, PWV, SD, SW, VP	Yao (2005)
Global	X	X	–	AOD, AT, D, GH, O, PWV, V, VV, OLR, WS	Graham et al. (2008)
South Pole	X	X	–	AI, AU, BL, FS, PWV, SB, ST	Saunders et al. (2009)
Chile	–	X	–	AT, BL, FS, OT, PWV, RH, WS	Vernin et al. (2011)
Australia	X	X	–	–	Hotan, Tingay & Glazebrook (2013)
Spain, Chile, Argentina	–	–	–	AT, BP, RH, WD, WS	Varela et al. (2014)
Turkey	X	X	X	AOD, PWV, WS	Aksaker et al. (2015)
MENA	X	X	X	AOD, AT, PWV, RH, WS	Abdelaziz et al. (2017)
Iran	X	X	X	AOD, IH, IF, LS, PWV, RH, S, SB, WS	Nasiri et al. (2019)
Pakistan	X	X	X	A, AOD, LU, LC, S, TS, WS	Daniyal & Hassan Kazmi (2019)

Table 2. Source, location and characteristics of datasets. Some datasets use more than one product. The resolution given here represents the original dataset; the final resolution is fixed to 1 km. Time coverage is usually taken from the satellite repositories. Two products of the Aqua/Terra satellites have different time coverage: 2000 February to date and 2002 to date for the MOD and MYD products, respectively. The time coverage of CC was started from 2003 July due to irregularities in earlier records from the MYD35_L2 product.

Layer	Satellite/instrument Resource Location	Product	Resolution	Coverage	Size
CC	Aqua/Terra-MODIS (NASA/LAADS DAAC) ladsweb.modaps.eosdis.nasa.gov/archive/allData/61/	MOD35_L2 MYD35_L2	1 km	2000–2019 2003–2019	24 TB
DEM	USGS – EROS Data Center (EDC) earthexplorer.usgs.gov	GTOPO30	1 km	1996	1.7 GB
AL	NOAA/SUOMI-NPP https://eogdata.mines.edu/download_dnb_composites.html	VIIRS/DNB	750 m	2016	25 GB
PWV	Aqua/Terra-MODIS (NASA/LAADS DAAC) ladsweb.modaps.eosdis.nasa.gov/archive/allData/61/	MOD07_L2 MYD07_L2	5 km	2000–2019 2002–2019	10 TB
AOD	Aqua/Terra-MODIS (NASA/LAADS DAAC) ladsweb.modaps.eosdis.nasa.gov/archive/allData/61/	MOD04_3K MYD04_3K MOD04_L2	3/10 km	2000–2019 2002–2019	24 TB
WIND	Model measurement globalwindatlas.info	Global Wind Atlas	225 m	2019	14 GB
LULC	Aqua/Terra - MODIS ladsweb.modaps.eosdis.nasa.gov/opendap/allData/6/MCD12Q1/contents.html	MCD12Q1	10 km	2018	200 MB

In all datasets (except AOD) not all time coverage was used; only twilight and night-time were selected. The reason for ignoring the daytime is simply because we aim to find clear skies during the night (optical telescopes work during the night-time). However, we have to also include twilight so as not to make discrete time spans in the dataset.

2.1 Cloud coverage (CC)

Cloud coverage or cloudiness is defined as the percentage of sky covered with clouds at the desired geographical coordinate (Glickman 2000). Note that astronomical observations rely on clear skies with almost no clouds in the sky. Therefore, CC is the first and the most important layer of astronomical site selection; see discussions in Graham et al. (2005), Sarazin et al. (2006), Varela et al. (2008), Aksaker et al. (2015). This fact can also be deduced from Table 1. CC can be recorded with many different methods: by synoptic naked-eye observations (Lau & Crane 1997; Bréon & Colzy 1999; Norris 1999), by using lidar and radar methods (Intrieri et al. 2002), by using an all-sky camera (Ackerman & Cox 1981; Pfister et al. 2003; Long et al. 2006) or using satellite monitoring (Venkatappa et al. 2019).

Since satellite data have good temporal and spatial resolution in determining cloud coverage we prefer it over the other methods. The MODIS (moderate-resolution imaging spectroradiometer) instrument has MOD35_L2 and MYD35_L2 cloud-coverage products that contain a cloud-mask layer. Global astronomical site selection should also take into account geographical conditions, climatic conditions and orography as well as the cloud coverage. Therefore atmospheric datasets should be sensitive to certain extreme conditions such as desert, snow, ice, altitude etc. (Ackerman et al. 1998; Frey et al. 2008).

The MODIS instrument provides 288 HDF4 files per day except for AOD. MODIS data are in HDF4 format (5-min granule size for a swath 2330 × 1354 km). An open-source PYTHON library was used to convert them into a GIS-suitable format. Conversion into GEOTIFF format according to the WGS84 DATUM criteria was handled by two PYTHON functions (WARP and TRANSLATE) of the GDAL (Geospatial Data Abstraction Library Virtual Format) library.

The cloud-mask data from MODIS consist of 48 bit pixel^{-1} information. Only the first eight bits are extracted and used in classifying the clear sky and the cloud detection (Platnick et al. 2003). The last bit of this extracted bit block determines whether a cloud-detection algorithm was used or not. The sixth and seventh bits of the block are used to introduce an index for CC. Since bitwise operation requires a lot of CPU power, parallel programming has been implemented in some parts of the code. Using this index a daily average has been calculated at each pixel. The long-term daily mean CC average was obtained by combining datasets of both the Aqua and Terra satellites. The resultant CC map is shown in Fig. 1.

Cloud dynamics show instantaneous variations that are mainly due to temperature, wind speed, wind direction and orography. However, on the global scale cloud circulations are due to the Earth's shape, rotation speed and direction, and depend on latitude. This global variation is also marked as northeasterly and southeasterly trade winds on Fig. 1.

Examination of CC reveals the following points on the global scale: a) clear night-sky (i.e. having less cloud coverage during night) counts are higher for western South and North America, north and north-west Africa and Australia than the rest of the world; b) some localized counts are due to climatological and geographical conditions; c) for western South America, South Africa and Australia, clear night-sky counts are due to the latitude effect; d) similarly, for the Northern hemisphere the latitude effect is generally less pronounced.

2.2 Digital elevation model (DEM)

Elevation (altitude) is also another important criterion in astronomical site selection. As the altitude of the site increases the site becomes less affected by atmospheric events such as clouds and aerosols, and therefore havs otentially good seeing values (Aksaker et al. 2015). Thus the best place will be above the atmosphere. DEM is a 3D model for visualizing the coordinate components of any topography and the differences in the altitudes. The DEM datasets are stored as raster-format digital images. The reference surface for any altitude point is generally taken as average sea level.

There exist many different resolutions for DEM, ranging from 30 m to 1 km. GTOPO30 with 1 km resolution DEM is used in this work. It has a horizontal grid spacing of 30″ (corresponding approximately to 1 km) and vertical units represent altitude in metres above mean sea level. It covers latitudes from 90°N to 90°S, and longitudes between 180°W to 180°E. The DEM dataset has 33 smaller pieces, or tiles in GEOTIFF format. The layer is given in Fig. 1.

2.3 Artificial light (AL)

Humanity has perturbed the world surface, as can be seen from space at night. The light created artificially increases the sky brightness, which is now defined as 'light pollution'. In a light-polluted region on the surface, the background of the sky increases and therefore the number of stars observed decreases exponentially. At the moment, one-third of humanity cannot see the Milky Way. Moreover, 80 per cent of the world lives in light-polluted regions (Falchi et al. 2016).

Astronomers look for sites with skies that are not polluted with artificial light. Thus, a night-time image of the Earth's surface will reveal dark regions as locations producing potentially less artificial light. Therefore, the collected night-time images will be the AL dataset.

The night-time data are from the Visible Infrared Imaging Radiometer Suite (VIIRS) day–night band (DNB), where DNB is in the visible band. The radiometric resolution of the dataset is up to 14 bits in visible to red wavelengths (0.5–0.9 μm) with radiation counts around 2×10^{-9} W cm^{-2} sr^{-1} (Nurbandi et al. 2016).

The dataset covers the world from 75°N to 65°S latitudes with 15″ grid size in a six-cell-set GEOTIFF format with a spatial resolution of 742 m pixel^{-1}. Night-time images are produced daily. However, Elvidge et al. (2017) filtered out non-artificial light sources (eg. lightning, fishing boats, clouds) and they created a database of images (monthly and yearly) on the website of the dataset. The dataset is ready to be used in GIS. Two different types are used: 1) extension 'vcm-orm-ntl' (the version with VIIRS cloud mask, outlier removed and night-time lights); 2) extension 'Avg_rade9' (brightness normalized with 10^{-9}). The layer is given in Fig. 1.

2.4 Precipitable water vapour (PWV)

PWV products of MODIS contain two different algorithms: a) near-infrared (daytime with 1 km spatial resolution); b) infrared (both day- and night-time with 5 × 5 km^2 spatial resolution). Since astronomical site selection concerns night-time sky conditions, infrared algorithms are preferred. Note that the MODIS atmospheric profile product (MOD07_L2 & MYD07_L2) also consists of other atmospheric datasets such as ozone, temperature profile, atmospheric stability and moisture profile.

The dataset contains 5-min swath images in version 6.1 (C6.1) in HDF4 format with 16-bit integer data type. The storage size is 288 files d^{-1}. Some days are missing in the dataset, which amounts to a maximum of 3 d yr^{-1}. PWV dataset has three subsets for the whole atmosphere: low, high, total. In this study, we only use the last one. The values of the dataset are in centimetres and the spatial resolution is 5 km.

As with the other MODIS products, PWV is converted to the WGS84 datum first, and then a mosaic is created later. They are stored in GEOTIFF format for further analysis in GIS. Using both satellites (Aqua and Terra), a mean PWV image was created for only night-time. Note that MODIS generates PWV values only for unclouded pixels. The layer is given in Fig. 1.

2.5 Aerosol optical depth (AOD)

AOD is defined as the total optical extinction in a column of atmosphere normally interpolated to 550 nm (Sayer et al. 2014).

AOD is directly related to the transparency of the sky. Two major entities, clouds and aerosols, degrade the transparency (Varela et al. 2008). Therefore, a lower annual AOD level will be good for an astronomical site.

In this study, the MODIS instruments on both the Aqua and Terra satellites were used. AOD products are produced using different algorithms for different contents, namely absence of cloud, snow and ice cover over land (using the Deep Blue and Dark Target algorithms) and ocean (using the Dark Target algorithm). The spatial resolutions of the AOD datasets are 10 × 10 km and 3 × 3 km for MOD04_L2 and MOD04_3K and MYD04_3K, respectively. Both datasets were used to obtain complete coverage.

MODIS delivers 288 HDF files per day. However, since AOD information is not produced at night, only ∼144 files are used. This is also applied to the AOD dataset with cloud coverage where AOD information is obtained from the land and ocean science dataset (SDS). All data were merged according to the WGS84 DATUM criteria and then converted to GEOTIFF format. The layer is given in Fig. 1.

2.6 Wind speed (WS)

High wind speed increases the kinematics of atmospheric particles, decreasing the stability of the atmosphere. It also indirectly affects the construction cost of the observatory dome. Therefore, annual lower wind speed is good for an astronomical site However, WS is a meteorological parameter that changes very rapidly from point to point. Note also that since wind causes atmospheric turbulence it is directly correlated with astronomical seeing (Liu et al. 2010).

The WS dataset used in this study was acquired from the World-Bank-supported project, Global Wind Atlas. WS was produced for a height of 10 m above the surface together with DEM and then reproduced with a resolution of 225 m. The datasets were combined with the mosaic method. The layer is given in Fig. 1.

2.7 Land use and land cover (LULC)

In an optimal astronomical site selection, the selection criteria should also include the following surface details: land use, land cover, water bodies, forest, agriculture land and barren lands.

The MODIS land-cover type product (MCD12Q1) provides a series of science datasets (SDSs) that map global land cover at 5 km spatial resolution in annual time steps for six land-cover types (Sulla Menashe & Friedl 2018). The MCD12Q1 product is created using a supervised classification of MODIS reflectance data (Friedl et al. 2002, 2010). The International Geosphere–Biosphere Programme (IGBL) legend and classification has also been adopted for this layer (table 3 of Sulla Menashe & Friedl 2018).

2.8 Other supplementary datasets

The country border data[1] is a vector format layer containing 247 regions as countries.

In total 2115 observatory locations[2] have been added. However, whenever available, they have been improved using the observatory's official website.

[1] http://thematicmapping.org/downloads/world_borders.php
[2] https://www.projectpluto.com/obsc.htm

3 GEOGRAPHIC INFORMATION SYSTEM (GIS)-BASED MULTI-CRITERIA DECISION ANALYSIS (MCDA)

In selecting an astronomical site, the analyst aims to determine an optimum location that would satisfy the selection criteria. Deciding on an appropriate astronomical site is based on numerous datasets (i.e. layers) collected according to criteria specific to astronomical sites. In deciding on a site to accommodate an observatory, the selection typically involves the evaluation of multiple criteria according to several, often conflicting, objectives (Rikalovic, Cosic & Lazarevic 2014). This can be dealt with by a key framework of GIS-based MCDA, which is considered to be an important spatial analysis method in the decision-making process that allows information derived from different sources to be combined (Feizizadeh, Jankowski & Blaschke 2014a).

GIS is designed as a system to capture, store, analyse and model the spatially referenced data to produce solutions to complex problems in many different fields (García-Cascales & Sánchez-Lozano 2013). The MCDA technique along with GIS can assist to categorize, examine and appropriately organize the collected information for spatial-based selection of astronomical sites.

In this study an MCDA method called simple additive weighting (SAW) by Churchman & Ackoff (1954) was used to assess the astronomical site-selection process. Since SAW uses weighted sums, it is accepted as one of the most applicable methods to deal with MCDA, especially under a GIS environment (Tzeng & Huang 2013). Therefore, we have used weighted criteria throughout the process. Then, the weight of each criterion layer was multiplied by the pixel-based importance score of the criteria. Therefore, the suitability index for astronomical sites (SIAS) can then be calculated using the following equation:

$$\mathrm{SIAS}_i = \sum_j W_j X_{ij}, \tag{2}$$

where SIAS_i is the index for pixel i, W_j is the relative weight for the jth criterion and X_{ij} is the importance score of pixel i for the jth criterion.

The MCDA framework for this study consists of three main stages:

(i) Spatial regulations: All criterion layers were transformed into a target spatial resolution of 1 km. The CC and AL layers were processed using the nearest-neighbour resampling method to decrease their original spatial resolutions of 3 km and 742 m to 1 km, respectively.

(ii) Standardization: Multiple criteria of SIAS cannot be compared or weighted without transforming each layer into a standardized common metric. Fuzzy sets have been applied using a sigmoidal function in order to standardize the criterion layers by assigning a degree of membership to each pixel of the criteria using an asymptotic scale from 0 to 1 (Jiang & Eastman 2000; Gorsevski & Jankowski 2010; Feizizadeh et al. 2014b).

(iii) Aggregation: In selecting suitable sites for an astronomical observatory, different types of datasets are combined with different types of criteria where at the end suitable locations can be subsetted from the global SIAS.

Overlay analysis is a spatial analysis technique used to merge and sum up all layers into a single layer by rescaling each layer to a common 0–1 scale. The overlay analysis within MCDA is called 'weighted averaging overlay', which is the sum of the standardized layers divided by the total weight. Therefore, overlay analysis is applied in our SIAS study.

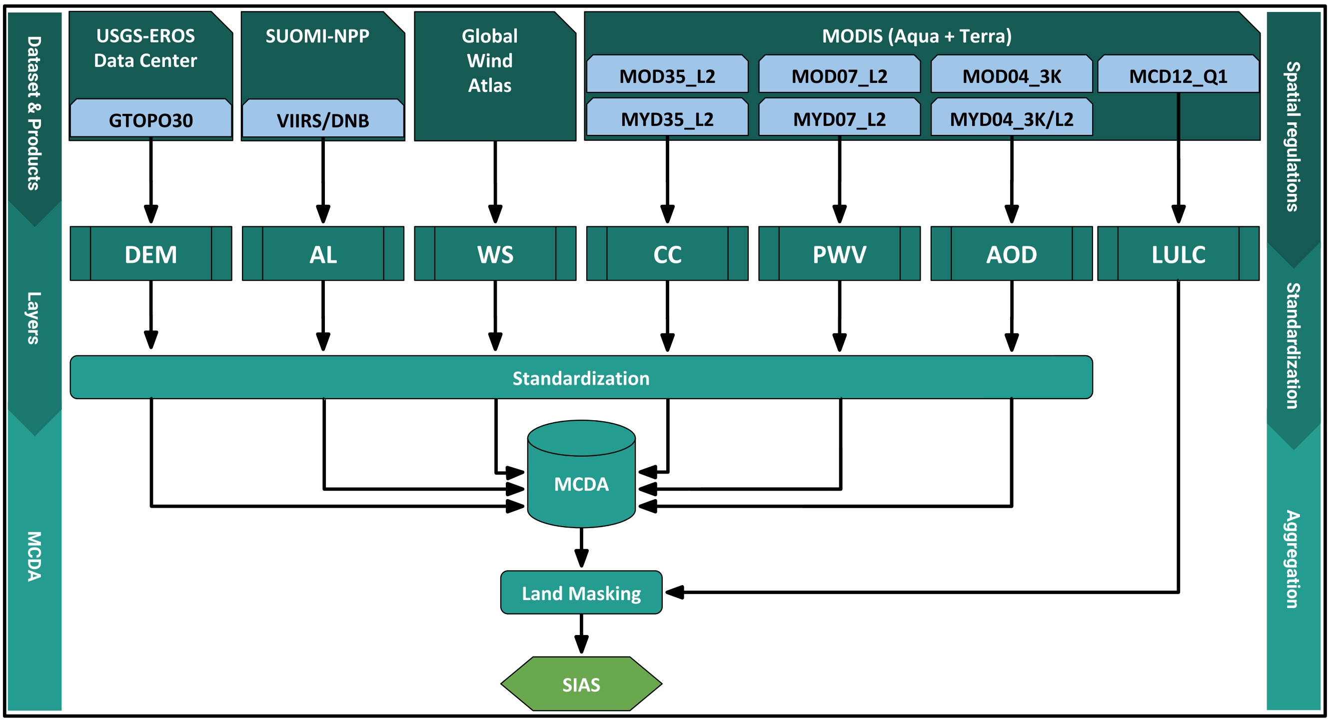

Figure 2. The pipeline of the site-selection process. See Section 3 for details.

Table 3. Summary of input and output of MCDA analysis for all the layers. AOD is a dimensionless number giving the total amount of aerosol within the vertical column over the site location. Since the final layer resolution is fixed to 1 km, the original resolution is given here. Definitions used in the Process column are as follows: NN: nearest-neighbour algorithm; LFZ: linear fuzzy logic; L: logarithm (base 10); SFL: S-shaped inverse sigmoidal fuzzy logic.

Layer	Original resolution (km)	Process		Layer value		Unit	Scale	
		IN	OUT	Min	Max		0 (worst)	1 (best)
CC	3	NN	LFZ	0.3	0.95	per cent	Cloudy	Clear
DEM	1	–	LFZ	−408	8685	m	Lowest	Highest
AL	0.375	NN	L + SFL	0	1682.71	W cm^{-2} sr^{-1}	Bright	Dark
PWV	5	NN	LFZ	0.68	53.54	mm	High	Low
AOD	3, 10	NN	LFZ	0	4.98	–	High	Low
WS	0.225	NN	LFZ	0.01	84.67	m s^{-1}	Fast	Slow
LULC	5	NN	–	–	–	CLASS	–	–

These processing steps were applied to all layers, except LULC. The pipeline of this analysis is given in Fig. 2. A summary is given in Table 3, and some additional notes are listed below:

(i) The values of the DEM dataset for global land areas were between −4941 and 8685 m. Values less than zero in terrestrial areas indicate errors due to the production process of the data. These incorrect values were rearranged according to the height of the Dead Sea, Israel (−408 m; the deepest terrestrial area in the world).

(ii) The values of the AL dataset range from 0–1683 W cm^{-2} sr^{-1}. The highest value of AL was recorded as 452 W cm^{-2} sr^{-1} in Las Vegas (USA). The dataset was skewed and it is corrected by using a logarithmic scale. Note that since illumination varies by the inverse square law, the logarithm of AL is used before it is fed into the SFL membership function. On this new scale, the average value of the dataset became −1.24.

(iii) Oceanic and sea areas were excluded from all datasets, leaving only the terrestrial surface area.

(iv) The values of the AOD dataset for the Sahara and Central Asian deserts were not covered in the 3 km resolution. Therefore, these regions are patched from 10 km resolution by resampling each pixel to 3 km.

3.1 SIAS series

A simple methodology is aimed in applying the MCDA analysis. The SIAS series created and layer weights are given in Table 4. In all series created, oceans are masked out; therefore, only terrestrial surface was included. Moreover, the Antarctica continent has been excluded (see Section 3). In addition to masking, using LULC's terrestrial identification, water surfaces within land (e.g. lakes, rivers etc.) were also excluded from the SIAS series.

Table 4. Series created by MCDA analysis for the layers discussed above. In each series a weight is given to each targeted layer. In all four series created, the layer lists of earlier works were modified in this work.

SIAS series	CC	DEM	AL	PWV	AOD	WS
A	1	1	1	1	1	1
B	1	1	1	–	–	–
C	2	1	1	–	–	–
D	1	2	1	–	–	–

Series A: A control series where the weights of all layers are equal. All six layers discussed above were included: CC, DEM, AL, PWV, AOD and WS. By doing so, a site's meteorological, geographical and anthropogenic properties are considered to be equal.

Series B: In this series, some of the correlated layers are excluded:

(i) PWV is highly correlated with altitude (Aksaker et al. 2015).

(ii) Astronomical observations usually work during the night. However, the AOD dataset has not been measured in the night-time (Remer, Tanré & Kaufman 2009) and it decreases as altitude increases, i.e. is correlated.

(iii) A limited number of global WS datasets exist: (a) The ERA5 model dataset[3] has a 31 km resolution; therefore it cannot be used in this study. (b) The World Bank's wind data were prepared together with DEM and reproduced with a resolution of 225 m. Although the resolution fits very well as a dataset it is excluded as a layer in this series to avoid DEM being used twice.

Therefore, as in Aksaker et al. (2015), only CC, DEM and AL are taken in this series.

Series C: A variation of series B: We increased the importance of CC to twice that of DEM and AL. Having less CC would mean that a site would have more observing time. Therefore, a location having a high SIAS series C value would be chosen as an observatory site, for example, running in queue mode or performing long-term surveys. This series will thus be called *observing time preferred*.

Series D: Another variation of series B: This time, the importance of CC and DEM are interchanged. Note that the seeing is highly correlated with the altitude (Racine 2005) (as the altitude increases the seeing values get better). Therefore, a location having a high SIAS series D value would be chosen for an observatory site, for example, working in the infrared band or expecting higher resolutions in both imaging and spectroscopy. This series will thus be called *seeing preferred*.

The world layout of each series along with its SIAS histogram are given in Fig. 3. Full country-based data access are available as supplementary material online.

4 RESULTS, CONCLUSION, DISCUSSION AND OUTCOMES

Using a GIS/MCDA analysis of seven different layers with an up-to-date coverage having a fixed 1 km spatial resolution for the entire terrestrial area, an index called the suitability index for astronomical sites (SIAS) is introduced for the first time. Datasets with 1 km spatial resolution correspond to approximately 1 gigapixel in size. Note that since PWV, AOD and WS are correlated with CC, DEM and AL, SIAS series A shows higher statistical values than series B, C and D. Therefore, it has to be taken as a control series. In total, four different SIAS series are created for different site-selection purposes.

Since the datasets cover several different wavelength bands, the outcome of this work will also be useful for other types of observatories working e.g. in radio astronomy. The statistical importance of the SIAS series can easily be gathered when SIAS values are analysed on a normal distribution (3σ rule). For each series the following are given in Table 5: (a) minimum, mean, maximum and σ values; (b) 1σ, 2σ and 3σ values; (c) corresponding land-surface area to these three σ levels and their percentages; (d) number of observatories falling into these three σ levels and their percentages.

4.1 Conclusions

The important outcomes of the four SIAS series are given below:

(i) First of all, we confirm the common sense of astronomical site-selection criteria: good sites can be sought around the tops of mountains (dark-green regions in Fig. 3).

(ii) If a site location is good enough (see discussion below) then it is found to be good in all four series. Therefore, the selected site status will be independent of the series (i.e. weights of the layers). Thus, one can select and use the output of a suitable series depending on the purpose of the selection.

(iii) Among all four series there is no single location on Earth with SIAS equal to 1.00. This is expected because naturally this value cannot be achieved under Earth's atmosphere.

(iv) A quick visual search of the results shown in Fig. 3 can be summarized as follows. The *best* locations with maximum SIAS values in all series, corresponding to regions with dark-green shading and $\geq 3\sigma$ level, are (a) the midwestern Andes in South America, (b) the Tibetan Plateau in western China.

(v) Similarly, *good* locations will have SIAS values corresponding to regions with light-green shading and 2σ level are (a) Greenland, (b) western North America, (c) Iran and the Arabian Peninsula, (d) western South America, (e) the northern, Middle Eastern and southern regions of Africa.

(vi) Therefore, the remaining SIAS values in all series can be thought of as the *worst* locations, corresponding to regions with yellow, orange and red shading and $\leq 1\sigma$ value.

(vii) Even though there is no obvious longitudinal localization on the SIAS values, there exist two latitude bands that can be marked as *good* or the *best*: one 10–50°N and the other 10–40°S. These regions are expected because they fall close to global cloud-circulation patterns of the Earth.

4.2 Discussion

(i) This work is limited to finding or localizing regions all around the terrestrial land surfaces, not to finding individual coordinates.

(ii) SIAS usage can be simplified by series B: Since some of the layers are correlated with the CC, DEM and AL layers, these three layers are found to be representative of all layers when astronomical site selection is targeted.

(iii) Since the resolution of layer datasets is finalized at 1 km, site selection cannot give definitive results (e.g. specific coordinates) unless datasets with finer resolutions are included (e.g. in metre

[3] https://confluence.ecmwf.int/display/CKB/ERA5

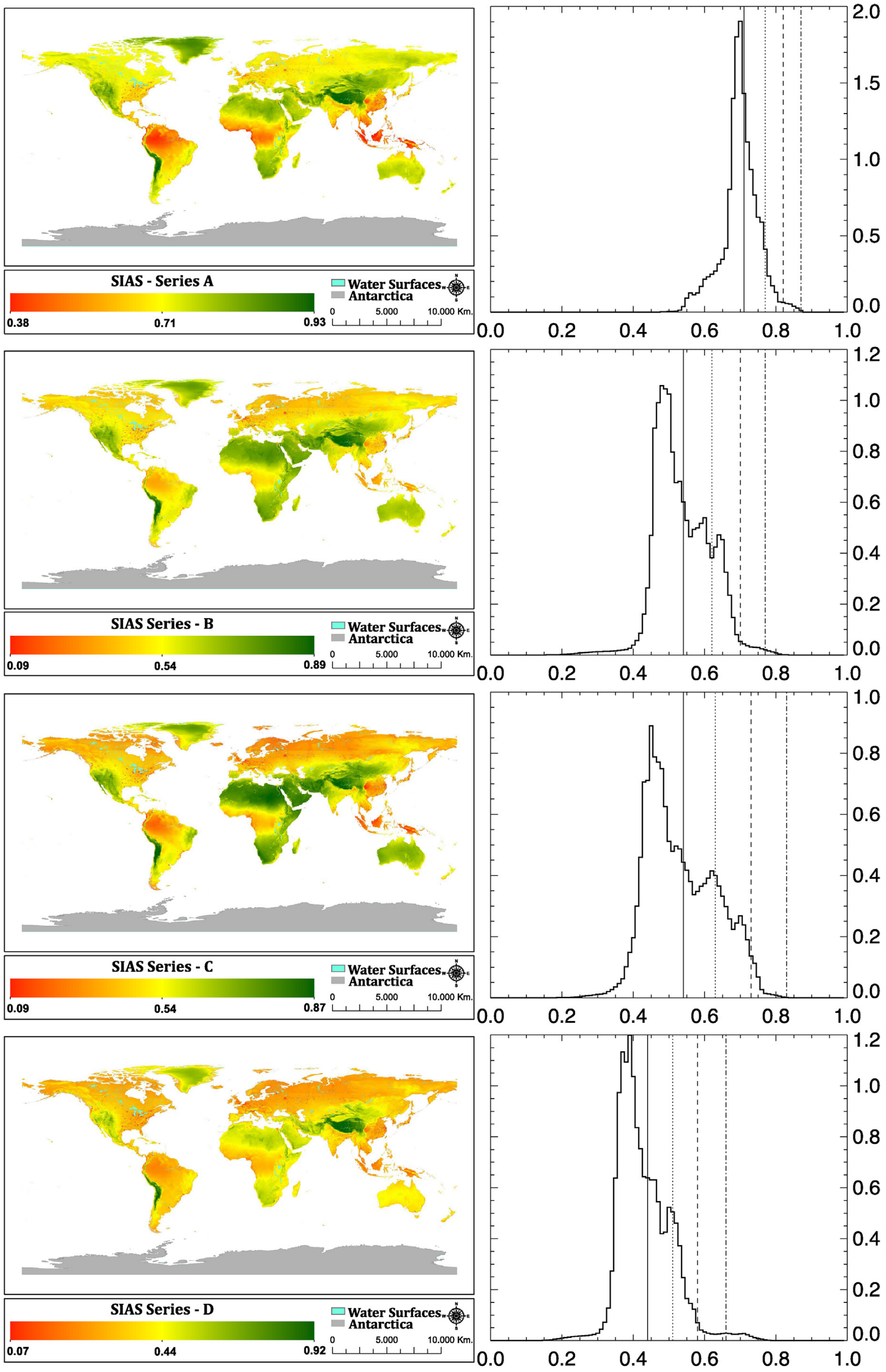

Figure 3. SIAS series created from GIS/MCDA analysis. Layouts (left column) of SIAS series A (top) to D (bottom) are given respectively, along with their histograms (right column). The frequencies of all histograms are normalized with 10^7. The histogram also includes the mean, μ (solid line), $\mu + 1\sigma$ (dotted line), $\mu + 2\sigma$ (dashed line), $\mu + 3\sigma$ (dash-dotted line). Statistical values are given in Table 5.

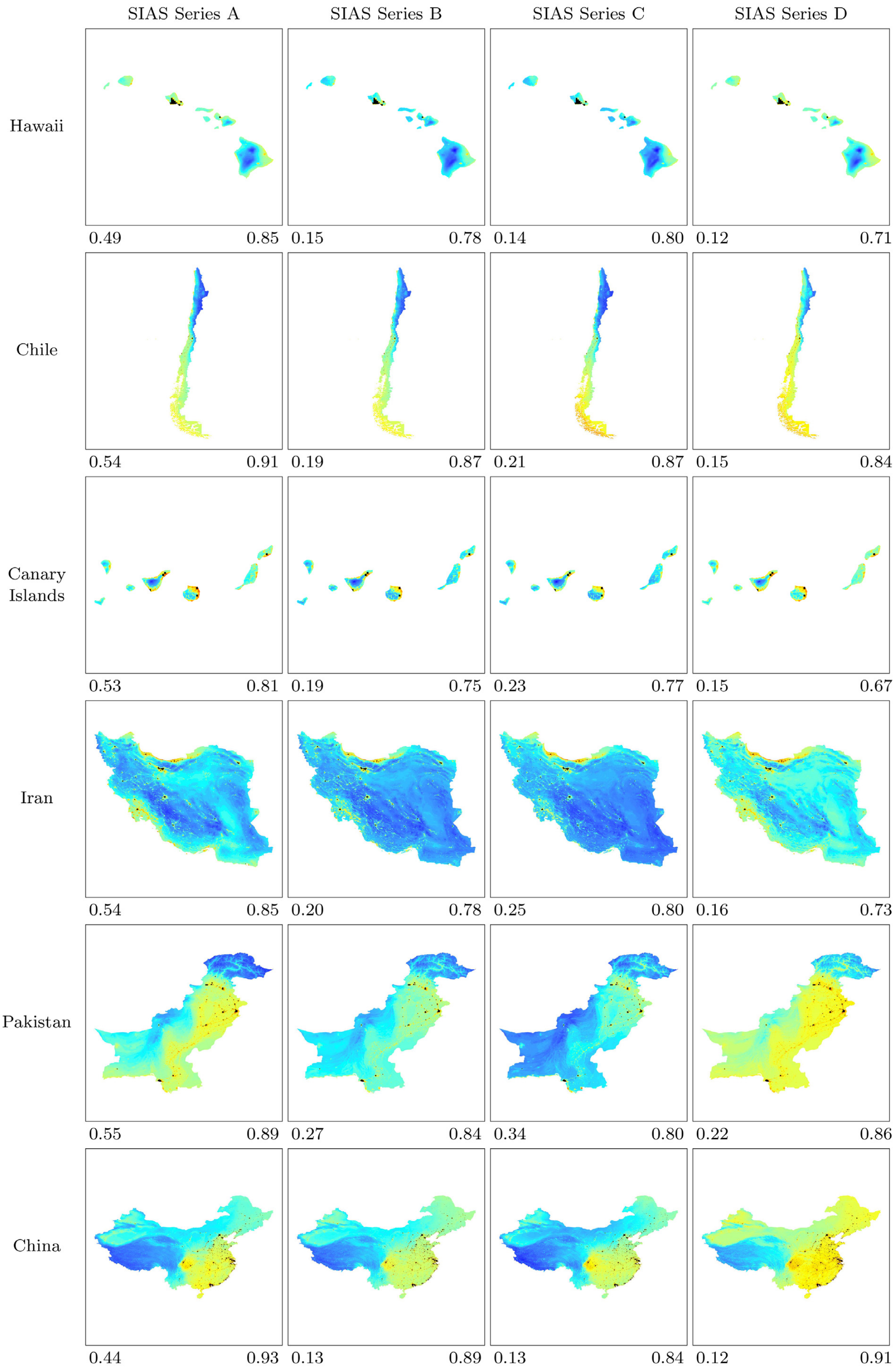

Figure 4. The results of a GIS/MCDA analysis in all series for a limited number of countries (top to bottom in longitude order): Hawaii, Chile, Canary Islands, Iran, Pakistan and China. SIAS series A–D are given from left to right. Minimum (left – red in colour grading) and maximum (right – blue in colour grading) values of each series are given below the corresponding map. Black represents built-up areas within the country. All country layouts will be available online.

Table 5. The statistics of the SIAS series. See Section 4 for explanation and details.

Series	Stat. of the series: Min	μ	σ	Max	Sigma level / Observatories (N) – ratio (per cent) / Surface area ($\times$ 10^6 sq km) – ratio to total land (per cent): $\mu + 1\sigma$		$\mu + 2\sigma$		$\mu + 3\sigma$	
A	0.38	0.71	0.05	0.93	0.77		0.82		0.87	
					205	9.66	37	1.74	3	0.14
					63.80	37.38	19.59	11.47	3.79	2.22
B	0.09	0.54	0.08	0.89	0.62		0.70		0.77	
					219	10.32	39	1.84	10	0.47
					43.26	25.35	27.87	16.33	3.67	2.15
C	0.09	0.54	0.10	0.87	0.63		0.73		0.83	
					235	11.07	43	2.03	1	0.05
					41.67	24.42	29.36	17.20	4.08	2.39
D	0.07	0.44	0.07	0.92	0.51		0.58		0.66	
					239	11.26	89	4.19	10	0.47
					45.18	26.47	22.53	13.20	5.13	3.01

Table 6. The results for a selected list of previous works on astronomical site selection. The table is in increasing publication year order. The AL layer is excluded because all of the selected observatory sites are located in dark regions (with AL values of 0.00). LULC identification numbers are taken from table 3 of Sulla Menashe & Friedl (2018). Regions from earlier studies: KALSU (western China); Shiquanhe (western China); OMA (western China); Chajnantor (Chile); Cerros Tolar (Chile); Cerro Armazones (Chile); Cerro Toloncharr (Chile); San Pedro Mártir (Mexico); Mauna Kea (Hawaii); Mt Meharry (Australia); Mereenie (Australia); ORM (Spain); Aklim (Morocco); Ventarrones (Chile); Macon (Argentina); Dinava (Iran); Gargash (Iran); Nok Kundi (Pakistan); Kalat (Pakistan); Kalam (Pakistan). References: [1] Yao (2005), [2] Sarazin et al. (2006), [3] Schöck et al. (2009), [4] Hotan et al. (2013), [5] Varela et al. (2014), [6] Nasiri et al. (2019), [7] Daniyal & Hassan Kazmi (2019).

Region Name	Ref.	λ	Φ	Layers: CC	DEM	PWV	AOD	WS	LULC	SIAS series: A	B	C	D
KALSU	[1]	74.80	38.15	0.31	4360	2.13	0.39	9.74	16	0.83	0.73	0.71	0.67
Shiquanhe	[1]	80.02	32.32	0.20	4788	1.9	0.25	6.93	16	0.87	0.78	0.78	0.73
OMA	[1]	83.07	32.55	0.24	4976	2.08	0.29	7.03	16	0.86	0.78	0.77	0.73
Chajnantor	[2]	– 67.75	23.02	0.13	5032	2.43	0.05	8.33	16	0.88	0.81	0.82	0.76
Cerro Tolar	[3]	– 70.09	– 21.96	0.07	2150	11.28	0.08	6.04	16	0.82	0.73	0.77	0.62
Cerro Armazones	[3]	– 70.18	– 24.58	0.05	2885	7.35	0.05	4.91	16	0.85	0.76	0.81	0.66
Cerro Toloncharr	[3]	– 67.97	– 23.93	0.13	4255	2.65	0.04	4.38	16	0.87	0.79	0.80	0.72
San Pedro Mártir	[3]	– 115.46	31.04	0.17	2657	15.15	0.12	4.78	10	0.79	0.71	0.74	0.62
Mauna Kea	[4]	– 155.48	19.83	0.14	3865	13.75	0.07	5.42	16	0.83	0.77	0.79	0.69
Mt Meharry	[4]	118.58	22.98	0.28	1100	18.93	0.01	6.49	7	0.73	0.62	0.63	0.50
Mereenie	[4]	132.20	23.88	0.25	790	15.75	0.00	6.48	7	0.75	0.61	0.64	0.49
ORM	[5]	– 17.89	28.76	0.28	2139	21.47	0.25	–	9	0.74	0.64	0.65	0.55
Aklim	[5]	– 2.43	34.91	0.38	146	17.34	0.11	4.28	12	0.71	0.55	0.56	0.43
Ventarrones	[5]	– 70.40	24.62	0.05	2528	9.50	10	5.69	16	0.83	0.75	0.80	0.64
Macon	[6]	– 67.78	22.93	0.14	5130	2.55	0.10	9.09	16	0.88	0.81	0.82	0.76
Dinava	[6]	50.54	34.09	0.24	1542	12.07	0.27	5.12	7	0.77	0.65	0.67	0.54
Gargash	[6]	51.31	33.67	0.24	3359	10.41	0.19	9.42	10	0.80	0.71	0.72	0.64
Nok Kundi	[6]	62.75	28.82	0.12	675	16.04	0.35	6.59	16	0.74	0.63	0.69	0.50
Kalat	[6]	27.70	27.70	0.14	1430	18.31	0.30	6.35	16	0.77	0.68	0.72	0.56
Kalam	[6]	34.00	34.00	0.27	610	18.37	0.59	4.83	10	0.72	0.61	0.63	0.49

order). Considering all the series, the 3σ level corresponds to ∼2–3 per cent of the land surface, which is equivalent to 3.5–5.0 million sq km. In size, this value is too big. Using a rough but quick calculation, tens of thousands of astronomical observatory sites could be found.

(iv) Therefore, the best way to use the SIAS series is to *eliminate* the worst ($\leq 1\sigma$), not to *find the best* ($\geq 3\sigma$). Moreover, the final site selection has to be done by performing long-term bottom-up on-site measurements.

4.3 Outcomes

Layouts of the SIAS series analysis are created for a total of 247 countries. However, countries with small land-surface area ($\leq$10 000 sq km) or countries with many small islands are excluded. Therefore, country layouts were created only for 168 countries. Among all the others, six countries were selected to compare the results of this work. They are either well known in observational astronomy or a recent site-selection study was performed on the site (westward longitude listed first): Hawaii, Chile, Canary Islands,

Table 7. The results for astronomical sites with a +4 m class telescope. The table is in decreasing latitude order from south to north. The AL layer is excluded because all of the selected observatories are located in dark regions (with AL values of 0.00), except MDO with an AL value of 49.5. LULC identification numbers are taken from table 3 of Sulla Menashe & Friedl (2018). Observatory (Obs.) abbreviations (the given geographic coordinates usually represent a single telescope among others): SAAO: South African Astronomical Obs.; CPO: Cerro Pachón Obs.; CTIO: Cerro Tololo Inter-American Obs.; LCO: Las Campanas Obs.; CA: Cerro Armazones.; PO: Paranal Obs.; MKO: Mauna Kea Obs.; ORM: Roque de los Muchachos Obs.; MDO: McDonald Obs.; FLWO: Fred Lawrence Whipple Obs.; KPNO: Kitt Peak National Obs.; MGIO: Mount Graham International Obs.; PalO: Palomar Obs.; LO: Lowell Obs.; DAG: Eastern Anatolia Obs.; BAO: Beijing Astronomical Obs.; SAO: Special Astrophysical Obs.; MRO: Maple Ridge Obs. The full observatory list will be available online.

Observatory			Layers							SIAS series			
Abbreviation	λ	Φ	CC	DEM	PWV	AOD	WS	LULC	A	B	C	D
SAAO	20.81	– 32.37	0.15	1640	9.71	–	7.57	2	0.80	0.68	0.72	0.57
CPO	– 70.73	– 30.24	0.19	2600	7.07	0.26	4.98	2	0.81	0.70	0.72	0.61
CTIO	– 70.80	– 30.16	0.18	1751	8.21	0.30	3.74	2	0.80	0.68	0.71	0.57
LCO	– 70.70	– 29.00	0.12	2144	7.48	0.26	3.48	2	0.82	0.71	0.75	0.60
CA	– 70.20	– 24.60	0.05	2789	7.35	0.06	4.74	16	0.85	0.77	0.81	0.66
PO	– 70.40	– 24.62	0.05	2374	9.50	0.10	5.99	7	0.83	0.74	0.79	0.63
MKO	– 155.47	19.82	0.14	4120	13.13	0.08	5.33	7	0.83	0.78	0.79	0.71
ORM	– 17.89	28.75	0.28	2214	21.47	0.25	5.57	4	0.74	0.65	0.66	0.56
MDO	104.02	30.67	0.30	1953	12.81	0.09	5.71	2	0.77	0.64	0.65	0.54
FLWO	– 110.88	31.68	0.30	2369	12.25	0.11	6.31	5	0.77	0.66	0.66	0.57
KPNO	– 111.59	31.95	0.27	1810	13.80	0.13	6.13	2	0.76	0.65	0.66	0.54
MGIO	– 109.89	32.70	0.29	3081	11.20	0.10	7.01	5	0.80	0.68	0.68	0.61
PalO	– 116.86	33.35	0.22	1676	14.20	0.09	2.77	4	0.77	0.66	0.68	0.55
LO	– 111.42	34.74	0.29	2330	9.43	0.06	3.23	9	0.79	0.66	0.67	0.57
DAG	41.23	39.78	0.36	2989	5.48	0.17	6.66	5	0.79	0.66	0.65	0.59
BAO	117.57	40.39	0.40	825	11.52	0.22	2.02	1	0.73	0.57	0.57	0.46
SAO	41.44	43.64	0.41	1995	8.48	0.09	4.77	8	0.77	0.61	0.59	0.52
MRO	– 122.57	49.28	0.60	356	11.89	0.17	1.47	1	0.69	0.47	0.45	0.37

Iran, Pakistan, China. The layouts of these regions are given in Fig. 4. Layouts for the other countries are are available as supplementary material online.

Due to the finalized resolution in the datasets, it would be wrong to label the whole country as best, good or worst just from the statistics of its SIAS series; localized best locations could be found in the worst regions. For example, in Hawaii and the Canary Islands, while the shores of the islands fall into the worst category, volcanic mountains and their caldera are in the best category. This is the same for Chile, China, Iran and Pakistan, where they have recently performed a site-selection study.

The SIAS series analysis for the observatories is given in Table 6. Using the 3σ rule given in Table 5, the following points are noted for the listed regions: (1) most are around or above 1σ in all of the series; (2) almost half of them are above the 2σ level in all of the series.

SIAS series analyses are also created specifically for 15 observatory sites with +4 m telescopes (in Table 7). Using the 3σ rule given in Table 5, the following points are noted for these observatories: (1) All are around or above 1σ in all of the series; (2) Most of them are also close to the 2σ level in all of the series.

In addition to this subset, the same analysis has been performed for all observatories, in total 2123. This is available as supplementary material online. When all of them are included, only approximately 10 per cent, 2.5 per cent, 0.3 per cent fall in the 1σ, 2σ, 3σ levels, respectively. However, to have complete statistics for current observatory sites, the database of the list has to be updated so that it only includes professional sites.

The most important outcome of this study is to create a suitability-index database for any terrestrial coordinate on Earth. This tabulated database will also contain all series studied in this work. Therefore, amateurs, institutions or countries aiming to construct an observatory could create a shortlist of potential site locations using SIAS values created for each country without spending time and budget.

The outcomes and datasets of this study have been made available through a website, the Astro GIS Database, at www.astrogis.org.

ACKNOWLEDGEMENTS

This research was supported by the Scientific and Technological Research Council of Turkey (TÜBİTAK) through project number 117F309. We thank Esragül Atalay, Derya Öztürk Çetni and Hülya Işık for their efforts in downloading datasets. We also thank the supervisors of the project, namely İbrahim Küçük, Süha Berberoğlu and Mustafa Atılan. We thank Mehmet E. Özel for his helpful comments. We thank Alisan Aktay for the design of the https://www.astrogis.org website.

The MOD35_L2 - MODIS/Terra Cloud Mask and Spectral Test Results 5-Min L2 Swath 250m and 1km, MYD35_L2 - MODIS/Aqua Cloud Mask and Spectral Test Results 5-Min L2 Swath 250m and 1km, MOD04_3K - MODIS/Terra Aerosol 5-Min L2 Swath 3km, MYD04_3K - MODIS/Aqua Aerosol 5-Min L2 Swath 3km, MOD04_L2 - MODIS/Terra Aerosol 5-Min L2 Swath 10km, MOD07_L2 - MODIS/Terra Temperature and Water Vapor Profiles 5-Min L2 Swath 5km and MYD07_L2 - MODIS/Aqua Temperature and Water Vapor Profiles 5-Min L2 Swath 5km dataset were acquired from the Level-2 and Atmosphere Archive & Distribution System (LAADS) Distributed Active Archive Center (DAAC), located in the Goddard Space Flight Center in Greenbelt, Maryland (https://ladsweb.nascom.nasa.gov/).

MCD12Q1 MODIS Land Cover Type Version 6 data product were acquired from the Level-3 and The Land Processes & Distribution System (LP) Distributed Active Archive Center (DAAC), located at the USGS Earth Resources Observation and Science

(EROS) Center in Sioux Falls, South Dakota (https://lpdaac.usgs.gov/).

Earth Resources Observation and Science Center/U.S. Geological Survey/U.S. Department of the Interior (1997): USGS 30 ARC-second Global Elevation Data, GTOPO30. Research Data Archive at the National Center for Atmospheric Research, Computational and Information Systems Laboratory.

Wind data obtained from the 'Global Wind Atlas 2.0, a free, web-based application developed, owned and operated by the Technical University of Denmark (DTU) in partnership with the World Bank Group, utilizing data provided by Vortex, with funding provided by the Energy Sector Management Assistance Program (ESMAP).

We acknowledge the product generation to the Earth Observation Group, Payne Institute for Public Policy.

REFERENCES

Abdelaziz G., Guebsi R., Guessoum N., Flamant C., 2017, J. Phys. Conf. Ser., 869, 012070
Ackerman S. A., Cox S. K., 1981, J. Applied Meteorology, 20, 581
Ackerman S. A., Strabala K. I., Menzel W. P., Frey R. A., Moeller C. C., Gumley L. E., 1998, J. Geophysical Res. Atmos., 103, 32141
Aksaker N. et al., 2015, Exp. Astron., 39, 547
Bréon F.-M., Colzy S., 1999, J. Applied Meteorology, 38, 777
Churchman C. W., Ackoff R. L., 1954, Operations Res., 2, 172
Daniyal A., Hassan Kazmi S. J., 2019, Res. Astron. Astrophys., 19, 129
Elvidge C. D., Baugh K., Zhizhin M., Hsu F. C., Ghosh T., 2017, Int. J. Remote Sensing, 38, 5860
Falchi F. et al., 2016, Sci. Advances, 2, e1600377
Feizizadeh B., Jankowski P., Blaschke T., 2014a, Comput. Geosciences, 64, 81
Feizizadeh B., Shadman Roodposhti M., Jankowski P., Blaschke T., 2014b, Comput. Geosciences, 73, 208
Frey R. A., Ackerman S. A., Liu Y., Strabala K. I., Zhang H., Key J. R., Wang X., 2008, J. Atmos. Oceanic Technol., 25, 1057
Friedl M. A. et al., 2002, Remote Sensing Environment, 83, 287
Friedl M. A., Sulla-Menashe D., Tan B., Schneider A., Ramankutty N., Sibley A., Huang X., 2010, Remote Sensing Environment, 114, 168
García-Cascales M. S., Sánchez-Lozano J., 2013, Renewable Sustainable Energy Rev., 24, 544
Glickman T. S., 2000, Glossary of Meteorology (2nd ed.). American Meteorological Society, Boston, MA
Gorsevski P. V., Jankowski P., 2010, Comput. Geosciences, 36, 1005
Graham E., Sarazin M., Beniston M., Collet C., Hayoz M., Neun M., Casals P., 2005, Meteorological Applications, 12, 77
Graham E., Sarazin M., Kurlandczyk H., Neun M., Matzler C., 2008, Proc. SPIE, 7012, 70121Y
Hellemeier J. A., Yang R., Sarazin M., Hickson P., 2019, MNRAS, 482, 4941
Hotan C. E., Tingay S. J., Glazebrook K., 2013, Publ. Astron. Soc. Australia, 30, e002
Intrieri J. M., Shupe M. D., Uttal T., McCarty B. J., 2002, J. Geophysical Res. Oceans, 107, SHE 5–1
Jiang H., Eastman J. R., 2000, Int. J. Geographical Inf. Sci., 14, 173
Küçük I. et al., 2012, Exp. Astron., 33, 1
Lau N.-C., Crane M. W., 1997, Mon. Weather Rev., 125, 3172
Liu L.-Y., Yao Y.-Q., Wang Y.-P., Ma J.-L., He B.-L., Wang H.-S., 2010, Res. Astron. Astrophys., 10, 1061
Long C. N., Sabburg J. M., Calbó J., Pagès D., 2006, J. Atmos. Oceanic Technol., 23, 633
Nas B., Cay T., Iscan F., Berktay A., 2009, Environmental Monitoring Assessment, 160, 491
Nasiri S., Darudi A., Khosroshahi H. G., Sarazin M., 2019, MNRAS, 486, 4226
Noorollahi Y., Yousefi H., Mohammadi M., 2016, Sustainable Energy Technol. Assessments, 13, 38
Norris J. R., 1999, J. Climate, 12, 1864
Nurbandi W., Ramadhani Yusuf F., Prasetya R. A., Dimas Afrizal M., 2016, in IOP Conf. Ser., Earth and Environmental Science, vol. 47. IOP Publishing, Bristol, p. 012040
Osborn J., Sarazin M., 2018, MNRAS, 480, 1278
Otarola A. et al., 2019, PASP, 131, 045001
Pfister G., McKenzie R. L., Liley J. B., Thomas A., Forgan B. W., Long C. N., 2003, J. Applied Meteorology, 42, 1421
Platnick S., King M. D., Ackerman S. A., Menzel W. P., Baum B. A., Riedi J. C., Frey R. A., 2003, IEEE Trans. Geoscience Remote Sensing, 41, 459
Racine R., 2005, PASP, 117, 401
Remer L. A., Tanré D., Kaufman Y. J., 2009, Algorithm for remote sensing of tropospheric aerosol from MODIS: Collection 5, Available at: https://modis-images.gsfc.nasa.gov/_docs/MOD04-MYD04_ATBD_C005.pdf
Rikalovic A., Cosic I., Lazarevic D., 2014, Procedia Eng., 69, 1054
Sarazin M., Graham E., Kurlandczyk H., 2006, Messenger, 125, 44
Saunders W. et al., 2009, PASP, 121, 976
Sayer A. M., Munchak L. A., Hsu N. C., Levy R. C., Bettenhausen C., Jeong M. J., 2014, J. Geophysical Res., 119, 13965
Schöck M. et al., 2009, PASP, 121, 384
Soltani A., Marandi I., 2011, J. Urban Environmental Eng., 5, 32
Sulla Menashe D., Friedl M. A., 2018, Technical report, User Guide to Collection 6 MODIS Land Cover (MCD12Q1 and MCD12C1) Product, Available at: https://modis.ornl.gov/documentation/guides/MCD12_User_Guide_V6.pdf
Tzeng G.-H., Huang J.-J., 2013, Multiple Attribute Decision Making Methods and Applications. Taylor and Francis, Oxford
Umar R., Zainal Abidin Z., Abidin Ibrahim Z., 2014, J. Phys. Conf. Ser., 539, 012009
Uyan M., 2013, Renewable Sustainable Energy Rev., 28, 11
van Belle G. T., Meinel A. B., Meinel M. P., 2004, SPIE Proc., 5489, 563
Varela A. M., Bertolin C., Muñoz-Tuñón C., Ortolani S., Fuensalida J. J., 2008, MNRAS, 391, 507
Varela A. M. et al., 2014, PASP, 126, 412
Venkatappa M., Sasaki N., Shrestha R. P., Tripathi N. K., Ma H.-O., 2019, Remote Sensing, 11, 1514
Vernin J. et al., 2011, PASP, 123, 1334
Yao Y., 2005, J. Korean Astron. Soc., 38, 113

SUPPORTING INFORMATION

Supplementary data are available at *MNRAS* online.

GSSA-Table7-Full.txt: Complete version of Table 7, values of six layers (CC, DEM, PWV, AOD, WS, LULC) and values of the four SIAS series (A, B, C, D) for all observatories.

GSSA-Figure4-Full.pdf: Complete version of Fig. 4, layouts of the four SIAS series (A, B, C, D) for all countries with surface area $>\sim 10$ km^2.

Please note: Oxford University Press is not responsible for the content or functionality of any supporting materials supplied by the authors. Any queries (other than missing material) should be directed to the corresponding author for the article.

This paper has been typeset from a TEX/LATEX file prepared by the author.